

Microstructure and micromechanical responses of bulk nanostructured high entropy alloy after heavy-ion irradiation at 500°C

Spencer Doran^a, Yonggang Yan^b, Liuqing Yang^c, Jae-Kyung Han^d, Di Chen^{e,f}, Kun Wang^b, Youxing Chen^c, Megumi Kawasaki^d, Tianyi Chen^{a,*}

^a School of Nuclear Science and Engineering, Oregon State University, United States

^b New York State College of Ceramics, Alfred University, United States

^c Department of Mechanical Engineering and Engineering Science, University of North Carolina, United States

^d School of Mechanical, Industrial and Manufacturing Engineering, Oregon State University, United States

^e Department of Physics & Texas Center for Superconductivity, University of Houston, United States

^f Idaho National Laboratory, P.O. Box 1625, Idaho Falls, ID 83415, United States



ARTICLE INFO

Keywords:

Nanocrystalline materials
Nanostructure
Coarsening
Severe plastic deformation
High entropy alloys

ABSTRACT

Nanocrystalline materials possess high defect-sink density, but often experience radiation-enhanced grain coarsening. With the intrinsic sluggish diffusion and radiation tolerance, high entropy alloys (HEA) may have superior radiation tolerance in their nanocrystalline form. In this study, CoCrFeNiMn HEA samples were processed via high-pressure torsion (HPT) under 6 GPa at room temperature for 1 (1T) and 8 (8T) turns to form nanograins with unsaturated and saturated plastic deformation, respectively. After 3.4MeV Ni ion irradiation at 500 °C, grain growth was observed in both HPT-processed samples. The microstructural evolution is dependent on pre-irradiation HPT processing, with the 8T sample showing stronger radiation tolerance against dislocation development and hardness changes, observed through transmission electron microscopy and nanoindentation, respectively. This radiation resistance is attributed to a unique nanodomain microstructure formed within the radiation-coarsened grains of the 8T sample. Microstructural and microchemical analysis suggested both HPT process and the alloy chemistry played roles in the nanodomain formation.

Nanocrystalline materials, characterized by a high grain boundary (GB) area-to-volume ratio, have great potential for application in radiation conditions where the accumulation of radiation-induced defects degrade the materials' properties and performance. It is well known that GBs and interfaces are effective defect sinks, suppressing defect accumulation [1–4]. However, many nanocrystalline structures, such as those introduced by severe plastic deformation (SPD), suffer from grain coarsening under thermal and irradiation conditions [4–10]. Thus, nanocrystalline materials have a low technology readiness level for nuclear application.

High entropy alloys (HEAs) show outstanding radiation tolerance. Under ion irradiation, coarse-grained HEAs have shown lower irradiation-induced swelling and suppressed damage formation [11–14]. Such radiation tolerance has been attributed to mechanisms such as sluggish diffusion, self-healing, and high lattice distortion [12]. Whether sluggish diffusion provides resistance of radiation induced segregation (RIS) remains an open question. Kumar et al. suggested

sluggish diffusion suppressing RIS through analytical comparison between ion-irradiated FeNiMnCr alloy and austenitic alloys of Fe-Cr-Ni and Fe-Cr-Mn, the former showing significantly lower RIS near grain boundaries [12]. However, Barr et al. reported same magnitude of segregation in CoCrFeNiMn HEA as Fe-Ni-Cr alloys after heavy ion irradiation at 500 °C, suggesting the preferential vacancy-solute based inverse Kirkendall effect mechanism that is not essentially suppressed by the increased number of elements in HEA alloys [15]. For a more comprehensive review of RIS and the mechanisms in HEA alloys, the readers are referred to Ref. [11].

The radiation tolerance of nanocrystalline HEAs has been investigated under ion and electron irradiations [4,6,10,16–18]. Nagase et al. reported no grain growth under MeV electron irradiation up to 40 displacements per atom (DPA) at up to 500 °C and suggested the important roles of GBs as defect sinks in impacting the irradiation-enhanced diffusion and facilitating irradiation-damage-healing [18]. Zhang et al. performed heavy-ion irradiation at room temperature up to 600 DPA

* Corresponding author.

E-mail address: Tianyi.chen@oregonstate.edu (T. Chen).

and observed the stability of the face-center-cubic (fcc) phase but a faster grain-growth kinetics under irradiation than that induced by thermal-annealing [4]. They suggested that disorder-driven grain growth under irradiation is more rapid than the grain rotation and GB migration mechanisms underlying the thermal-induced grain growth [4]. The disorder-driven grain-growth mechanism was also attributed for the rapid initial grain growth of nanocrystalline HEAs under in-situ transmission electron microscopy (TEM) ion irradiation by Zhou et al. [10], who reported that the grain-growth kinetics correlate negatively with the cohesive energy depending on the alloy composition [10].

In this study, bulk CoCrFeNiMn HEAs were produced by Powder Bed Fusion (PBF) technology and processed by high-pressure torsion (HPT) under 6 GPa and at one rotation per minute for nanograins refinement. Sample grains were refined from approximately 1–2 μm to dozens of nanometer grains [19,20]. Three sample conditions, undeformed, 1-turn, and 8-turn HPT processed, referred as 0T, 1T, and 8T, respectively, were selected in this work to compare their radiation responses. The samples were polished using a series of silicon carbide grit papers and finished with 0.05 μm diamond/alumina-polishing suspension to create a mirror surface.

Ion irradiation was performed at 500 °C. This temperature was chosen to not allow thermal relaxation of the nanograins. Resistance against grain coarsening under thermal annealing has been observed to be greater than 700 °C for the same material [6,21,22]. Defocused nickel ions of 3.4 MeV with a flux of $6.25 \times 10^{12} \text{ ions}\cdot\text{cm}^{-2}\text{s}^{-1}$ were used to produce a total fluence of $1.019 \times 10^{17} \text{ ions}\cdot\text{cm}^{-2}$. Stopping and ranges of ions in matter (SRIM) simulation was performed using the Kinchin-Pease (K-P) model, with the displacement energy being 40 eV [13,23]. As shown in Supplementary Fig. 1, a peak and an average DPA of 173 and 100 were received by the sample at a depth of 1080 nm and 550 nm, respectively. The change in composition percentage of Ni by the implanted ions is quantified by the implanted Ni concentration / original Ni concentration to show that the implanted ions should not cause phase instabilities. We focus our analysis between 200 and 800 nm to minimize both surface and implanted ion effects [24].

TEM was performed to investigate the microstructure evolution under irradiation. Thermo Fisher Scientific (FEI) SciosTM 2 DualBeam ultra-high-resolution analytical FIB-SEM system was used to prepare the cross-sectional transmission electron microscopy (TEM) specimens from the irradiated surface. The thickness of lamella was approximated to be 100 nm via SEM. Thermo Fisher Scientific (FEI) Talos F200X TEM with nano-diffraction capability was used in both conventional bright field

TEM mode and scanning TEM (STEM) mode to investigate grain size of the post-irradiated HEA samples and radiation induced defects.

The nanoindentation hardness was measured on Agilent Nano-Indenter G200 (MTS) with a Berkovich tip. The Continuous Stiffness Measurement (CSM) method based on the Oliver-Pharr method was chosen to record hardness as a function of penetration depth [25]. Multiple indents were performed on each sample, within the irradiated and unirradiated areas.

The nanohardness with and without irradiation were compared in Fig. 1. The 0 turn sample shows irradiation hardening, whereas the 1T and 8T samples reduce their hardness by 38.18% and 17.1%, respectively. A plateau was observed around 100 to 150 nm in the hardness profiles for the unirradiated 1T and 8T samples, both developed nanocrystalline grains due to HPT. The plateaus are attributed to the hardening effects of the nanograins, which disappear after irradiation. Quantitative analysis of the hardness changes with and without irradiation is based on the hardness value taken from the depth between 200 and 350 nm. This depth was selected to better represent the hardness changes by irradiation, without the interference from the unirradiated materials underneath. Such interference can be indicated by the tailings of the curves in Fig. 1b.

In Fig. 2, TEM images showed irradiation-induced grain coarsening in 1T and 8T samples. The irradiated zones of the 1T and 8T samples were transformed into large grain layers, which contain grains of 220 ± 20 and 210 ± 40 nm diameters for the 1T and 8T samples, respectively. The above mean grain sizes were determined in the range of 200 to 800 nm from the surface to avoid the surface and implanted ion effects in ion-irradiated samples. It is worth mentioning that the coarsened grains in the HPT samples are still smaller than the grains in the 0T sample, as shown in Fig. 2(a-c) and Table 1.

Fig. 2(d-f) display the irradiation-induced dislocation structures in the 0T, 1T, and 8T samples, respectively. Dislocation networks were observed in the 0T sample whereas loops around 20 nm in diameter were observed in the 1T and 8T samples, respectively. The statistics of dislocation network density and dislocation loops are presented in Table 1. The dislocation loops in the 8T sample are slightly finer than those in the 1T sample.

A closer look into the irradiated 8T sample via high-angle annular dark-field (HAADF) TEM revealed the development of nanodomains in the coarsened grains, as shown in Fig. 3(a). This pattern was not observed in the irradiated 0T or 1T samples. At higher magnifications in Fig. 3(b), the nanodomains show different contracts, whose nano-

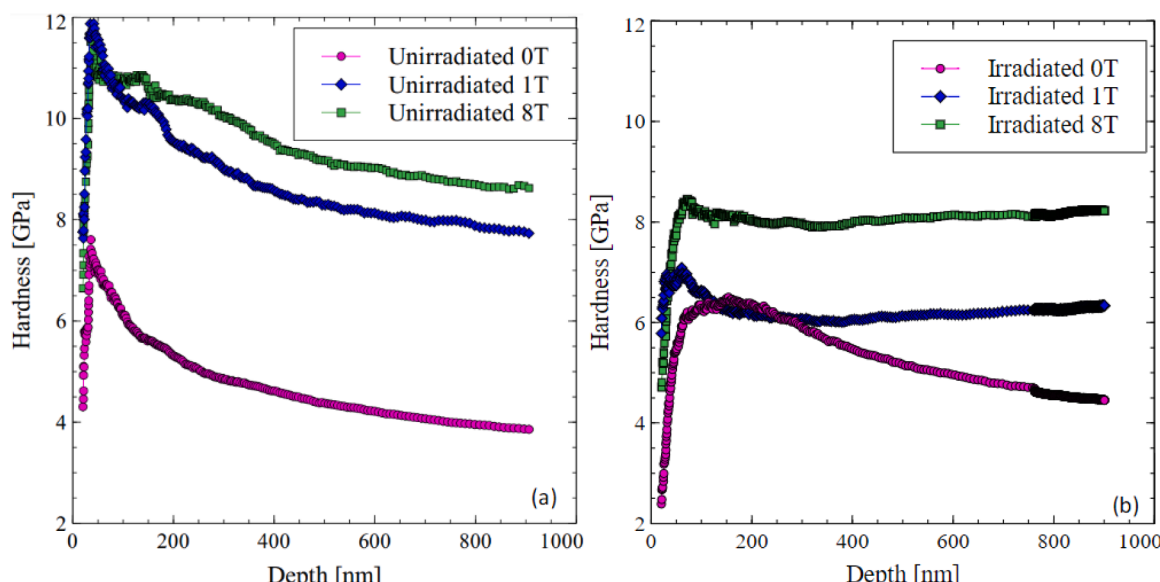


Fig. 1. Representative hardness curves of the 0T, 1T, and 8T samples before (a) and after (b) irradiation.

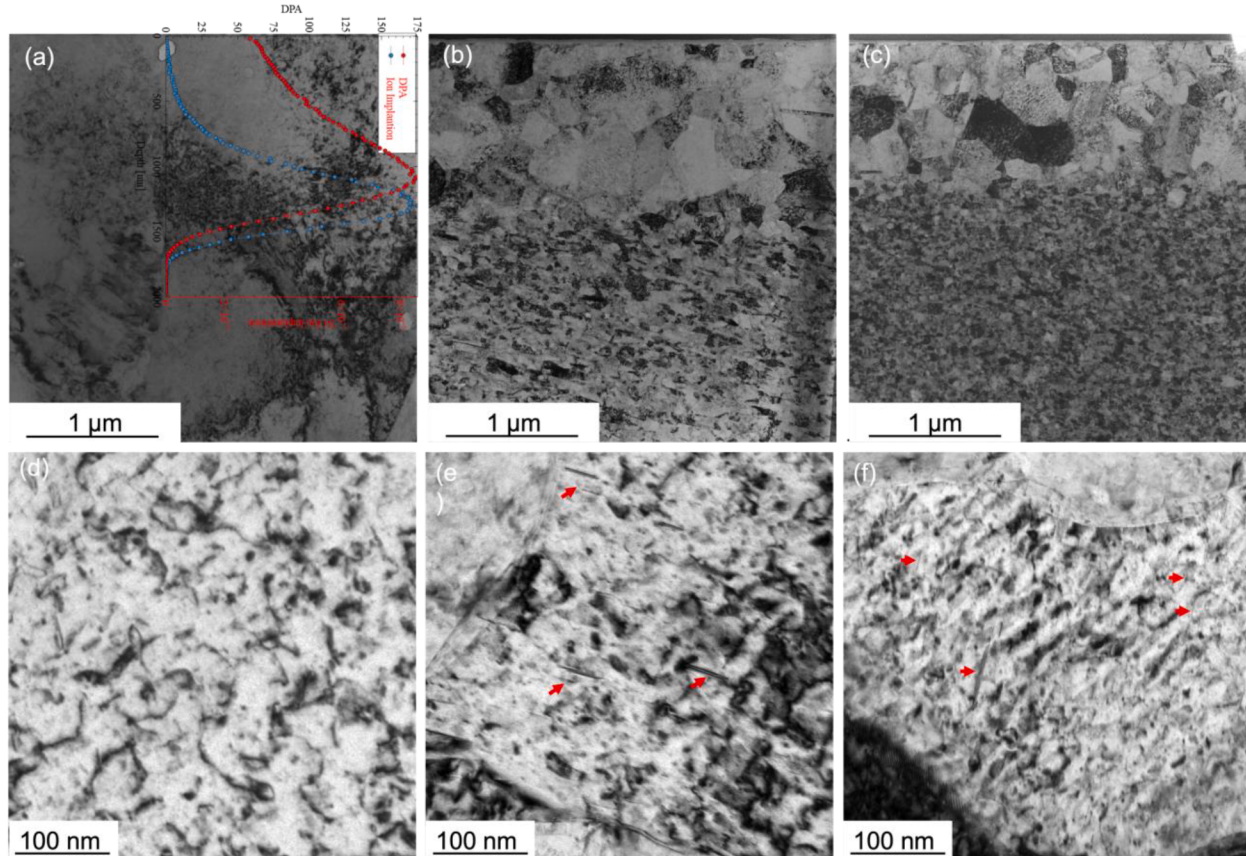


Fig. 2. Low-magnification TEM images showing grain structures in the irradiated 0T, 1T, and 8T samples in (a-c), respectively, with the damage and implanted Fe profiles superimposed; and high-magnification TEM images showing irradiation-induced dislocation structures in the 0T, 1T, and 8T samples in (d-f), respectively. Superimposed on (a) is the SRIM simulation showing the radiation damage (blue) and implanted ion (red) distribution, scaled to the TEM image. The readers are referred to Supplementary Fig. 1 for better readability of the SRIM plots. (For interpretation of the references to colour in this figure legend, the reader is referred to the web version of this article.)

Table 1

Experimentally determined microstructural and micromechanical characteristics and the microstructure-based hardness prediction by combining Hall-Petch and dispersed barrier models.

		0T	1T	8T
Unirradiated condition	Grain Size (nm)	1100 ± 200	63±5	45±4
	Hardness (GPa)	4.4 ± 0.1	8.4 ± 0.3	9.3 ± 0.3
Irradiated condition	Grain Size (nm)	unchanged	220±20	210±40
	Dislocation Loop Size (nm)	N/A	24±4	18±2
Microstructure-based hardness prediction	Dislocation Density	Network: $2.8 \times 10^{14} / m^2$	Loops: $1.9 \times 10^{21} / m^3$	Loops: $2.5 \times 10^{21} / m^3$
	Hardness (GPa)	6.0 ± 0.7	6.1 ± 0.8	8.0 ± 0.4
Hall-Petch Hardness (GPa)	4.4 ± 0.7	6.0 ± 0.6	6.0 ± 0.7	
Dislocation Hardness (GPa)	1.1 ± 0.1	0.90±0.07	0.82±0.05	
Total Hardness (GPa)	5.6 ± 0.8	6.9 ± 0.7	6.8 ± 0.7	

diffraction patterns, obtained near to the [011] zone, are displaced in Fig. 3(c-e). The shifting of the [011] zone shows the small-angle misorientation between the nanodomains, which is estimated to be on the order of 5°.

Fig. 3 (f-j) display the chemical composition maps of the region of Fig. 3(b). Nanoscale chemical segregation, not presented before irradiation, was observed after irradiation in the 8T sample. Enrichments of Co and Ni are accompanied by depletion of Cr and Fe, while Mn remains uniform. This segregation does not lead to phase instability as new phases are not observed by the diffraction patterns nor suggested by thermodynamics [26]. On the other hand, this microchemical fluctuation is spatially correlated to the nanodomain features observed in Fig. 3 (b).

The microstructural input was provided to the Hall-Petch and dispersed barrier hardening models to estimate the hardness of the irradiated samples. The model predictions are provided in Table 1 and visualized in Fig. 4. The models' details are as follows. For the 0T sample, dislocation network hardening was estimated by the dispersed barrier model [27]:

$$\Delta\sigma_y = Ma\mu b\sqrt{\rho} \quad (\text{Eq. (1)})$$

where b is the burgers vector, M the Taylor Factor ($M = 3$ for fcc), μ the shear modulus ($\mu = 80$ GPa) [28]. When considering the hardening by dislocation loops, the same formula is used by letting $\rho = Nd$, where N and d are the number density and loop size, respectively. For the HPT-processed samples, the irradiation-induced softening, attributed to the grain coarsening, is captured by the Hall-Petch relationship, Eq. (2) [29], and partially offset by the development of dislocation loops,

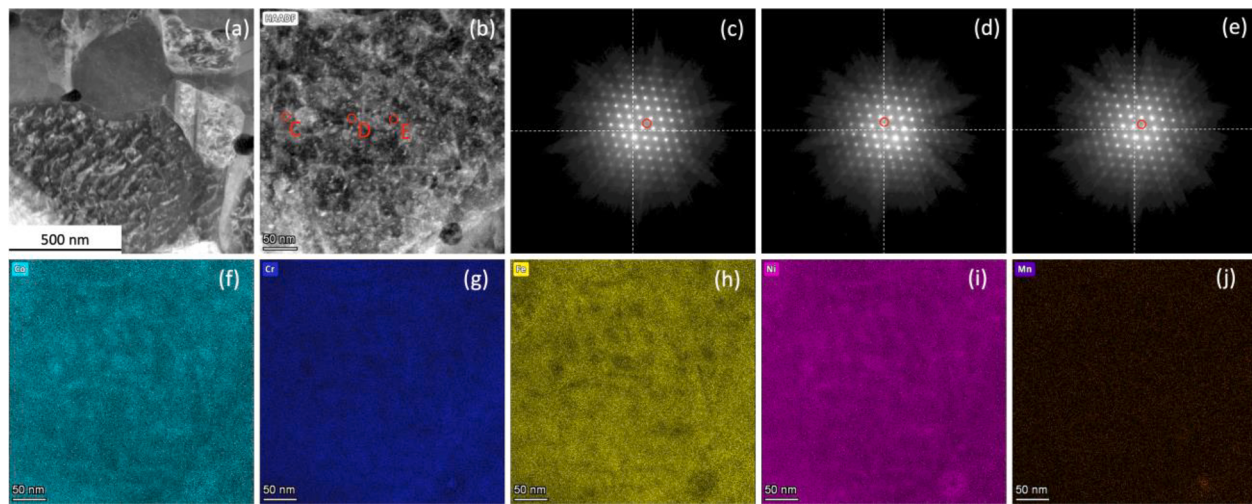


Fig. 3. Nanodomains observed in the irradiation-coarsened grains of the 8T sample at low (a) and high (b) magnifications. The nano-diffraction patterns at the spots labeled as C, D, and E in (b) were presented in (c), (d), and (e), respectively, with the [011] zone marked by red circles. The chemical composition maps of Co, Cr, Fe, Ni, and Mn were presented in (f-j), respectively. (For interpretation of the references to colour in this figure legend, the reader is referred to the web version of this article.)

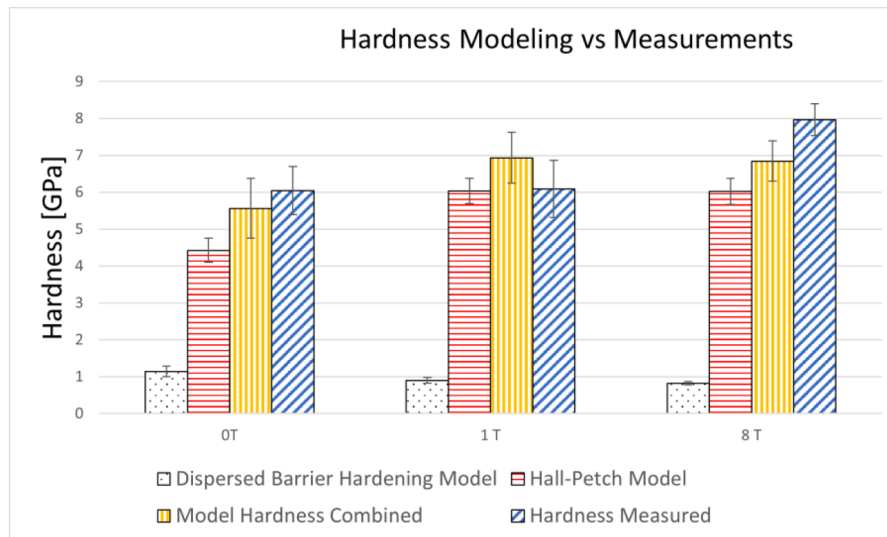


Fig. 4. Hardness predictions by combined dispersed barrier hardening and Hall-Petch models in comparison with the experimentally measured values.

$$\sigma_y = \sigma_0 + \frac{k_y}{\sqrt{d}} \quad (\text{Eq. (2)})$$

where σ_y is the measured hardness, and d is the grain size. The Hall-Petch parameters, σ_0 and k_y , were fitted using the hardness and grain size data before irradiation of 0T, 1T, and 8T samples, to be 3.2 ± 0.2 GPa and 41 ± 3 GPa nm $^{1/2}$, respectively. The fitted Hall-Petch model was then used to estimate the GB contribution to the hardness of the irradiated samples, taking the grain coarsening data in Table 1 as input. Dislocation loop hardening was calculated using Eqn. (1). The strength factor α was determined using Tan and Busby's formula [27]. The sums of microstructure-dependent hardening determined by the Hall-Petch and dispersed barrier-hardening models were compared with the measured hardness in Fig. 4. The uncertainties of the modeled hardness values were propagated from the standard errors of the mean of the microstructural measurements. The error bar of the measured hardness represents the standard error of the mean of the CSM hardness among 4–6 measurements for each sample.

As shown in Fig. 4, the modeled hardness is in good agreement with

the experimental measurements, especially for 0T and 1T samples. However, the comparison between 1T and 8T samples implies that the sum of the GB and dislocation loop hardening underestimates the hardness of the 8T sample. Although the two samples show similar irradiation-induced grain coarsening and dislocation, the measured hardness of the irradiated 8T sample is systematically higher than that of the irradiated 1T sample. This hardness difference is attributed to the sub-grain nanodomains shown in Fig. 3, which is estimated to have a hardness contribution on the order of 1 GPa. The nanodomains in the irradiated 8T sample present a high density of small-angle boundaries serving as dislocation barriers [30]. Neither such nanodomains nor the chemical segregation (Fig. 3f-j) was observed in the 1T sample. Comparison of the irradiated microstructures between the 1T and 8T samples indicates that the saturated plastic deformation in the 8T sample may be necessary for the formation of this nanodomain feature, possibly through the micro-segregation which introduces lattice mismatches that are accommodated by the small-angle boundaries.

This study showed that the nanocrystalline grains produced by HPT in HEA are not stable under ion irradiation at 500 °C. Comparing the

irradiated zone and the thermal-annealed zone, one notices that the grain growth is significant in the former but negligible in the latter. This comparison suggests that the grain coarsening is radiation-induced rather than radiation-enhanced. Zhang et al. showed radiation-induced grain growth in nanocrystalline HEA even at room temperature and suggested disorder-driven grain growth as a possible mechanism that is more rapid than the thermal processes of grain rotation and GB migration[4]. Coherent observations and conclusions were made via in-situ TEM irradiation by Zhou et al. [10]. Such an athermal mechanism provides a possible explanation for the radiation-induced grain growth observed in this study.

Despite grain coarsening under irradiation, the HPT-processed samples show enhanced radiation tolerance evidenced by the suppressed dislocation development. Unlike the unprocessed sample developing dislocation networks under irradiation, the HTP-processed samples show dislocation loops of around 20 nm. The size of dislocation loops decreases with increasing HPT turns. At the irradiation temperature of 500 °C, dislocation networks are generally observed in ion-irradiated solid-solution alloys at relatively low DPA, as a result of the growth, unfaulting, and coalescing of dislocation loops. This dislocation evolution is suppressed in HEAs thanks to the intrinsic sluggish diffusion [12,13]. For example, Kiran Kumar, et al. reported limited increases in loop size between 400 and 700 °C in ion-irradiated HEA alloys up to 10 DPA to illustrate the sluggish diffusion in HEAs promoting point defect recombination. In the current study, we showed that HEAs develop dislocation networks at 100 DPA with a density of $2.8 \times 10^{14} /m^2$. On the other hand, the HPT processes effectively suppressed the development of dislocation structures and thus are expected to enhance the radiation resistance of HEAs. It is also worth noting that increasing the number of HPT turns enhances the effect of dislocation loop suppression, as seen by the comparison between the 1T and 8T samples in Table 1.

The sub-grain domains observed in the irradiation-coarsened grains of the 8T samples (Fig. 3) provide additional defect sinks and dislocation barriers, which may suppress the growth of dislocation loops (Fig. 2 and Table 1) and alleviate the radiation-softening due to grain coarsening (Fig. 1). The fact that such sub-grain microstructure was observed in the 8T sample but not in the 1T sample indicates the effects of plastic deformation saturation on the microstructural stability of the SPD features in HEAs. Prior studies by Hung et al. and Gubicza et al. showed that the saturation of plastic deformation occurs in the HEA after 5 turns of the HPT process [19,31]. This saturation is characterized by GB structure relaxation and the formation of nanostructures inside the nanocrystalline grains [21,32–34]. Comparison between the radiation responses of the 1T (unsaturated) and 8T (saturated) samples indicate that the signatures of strain saturation preserve even after irradiation-induced grain coarsening in the HEA. Although the formation mechanism of the sub-grain microstructure is beyond the scope of this study, it is speculated that both the saturated characteristics of the initial HPT-processed microstructure and the specific chemical composition of this HEA play roles in the formation of this novel microstructure. It is possible that the saturated severe deformation has introduced defect sinks of specific characteristics that facilitate RIS to form the nanoscale chemical segregation (Fig. 3), which stabilizes the nanodomain structure. Whether this nanodomain structure is stable against further irradiation remains an open question. Future modeling and advanced experimental studies (such as those utilizing in-situ ion-irradiation TEM) are expected to shed light on the mechanisms of the preservation of SPD signatures in HEAs under irradiation.

In summary, this study showed radiation-induced grain growth in HPT processed CoCrFeNiMn HEAs following 3.4 MeV Ni ion irradiation at 500 °C up to 100 DPA. Despite the instability of the HPT-induced nanocrystalline grains, the HPT processes extend the radiation resistance of the HEAs, evidenced by the suppression of dislocation development. A novel sub-grain microstructure was observed in the irradiation-coarsened grains of the HEA samples processed by HPT to saturated plastic deformation (after 8 turns). This observation provides

the microstructural basis of the extended radiation tolerance (both dislocation suppression and reduced softening) and the potential longevity of the effects of SPD in HEAs under irradiation.

Declaration of Competing Interest

The authors declare that they have no known competing financial interests or personal relationships that could have appeared to influence the work reported in this paper.

Acknowledgment

This study was supported in part by the National Science Foundation of the United States under grant no. DMR-1810343. The Thermo Fisher Scientific (FEI) SciosTM 2 DualBeam ultra-high-resolution analytical FIB-SEM at Alfred University system is supported by the National Science Foundation under grant no. 2018306. Spencer Doran acknowledged the Department of Energy, Office of Nuclear Energy for the Integrated University Program Scholarship and the University Nuclear Leadership Program Scholarship, and the Society of Mining, Metallurgy, and Exploration for the WAAIME Scholarship. Tianyi Chen acknowledged the support of the start-up funds by Oregon State University.

Supplementary Materials

Supplementary material associated with this article can be found in the online version, at doi:10.1016/j.scriptamat.2023.115628.

References

- [1] X. Zhang, K. Hattar, Y. Chen, L. Shao, J. Li, C. Sun, K. Yu, N. Li, M.L. Taheri, H. Wang, J. Wang, M. Nastasi, Radiation damage in nanostructured materials, *Prog. Mater. Sci.* 96 (2018) 217–321, <https://doi.org/10.1016/j.pmatsci.2018.03.002>.
- [2] M. Song, Y.D. Wu, D. Chen, X.M. Wang, C. Sun, K.Y. Yu, Y. Chen, L. Shao, Y. Yang, K.T. Hartwig, X. Zhang, Response of equal channel angular extrusion processed ultrafine-grained T91 steel subjected to high temperature heavy ion irradiation, *Acta Mater.* 74 (2014) 285–295, <https://doi.org/10.1016/j.actamat.2014.04.034>.
- [3] T. Chen, E. Aydogan, J.G. Gigax, D. Chen, J. Wang, X. Wang, S. Ukai, F.A. Garner, L. Shao, Microstructural changes and void swelling of a 12Cr ODS ferritic-martensitic alloy after high-dpa self-ion irradiation, *J. Nucl. Mater.* 467 (2015) 42–49, <https://doi.org/10.1016/j.jnucmat.2015.09.016>.
- [4] Y. Zhang, M.A. Tunès, M.L. Crespillo, F. Zhang, W.L. Boldman, P.D. Rack, L. Jiang, C. Xu, G. Greaves, S.E. Donnelly, L. Wang, W.J. Weber, Thermal stability and irradiation response of nanocrystalline CoCrCuFeNi high-entropy alloy, *Nanotechnology* 30 (2019), 294004, <https://doi.org/10.1088/1361-6528/ab1605>.
- [5] D. Kaoumi, A.T. Motta, R.C. Birtcher, A thermal spike model of grain growth under irradiation, *J. Appl. Phys.* 104 (2008), 073525, <https://doi.org/10.1063/1.2988142>.
- [6] Q. Lin, X. An, H. Liu, Q. Tang, P. Dai, X. Liao, In-situ high-resolution transmission electron microscopy investigation of grain boundary dislocation activities in a nanocrystalline CrMnFeCoNi high-entropy alloy, *J. Alloys Compd.* 709 (2017) 802–807, <https://doi.org/10.1016/j.jallcom.2017.03.194>.
- [7] J.G. Gigax, H. Kim, T. Chen, F.A. Garner, L. Shao, Radiation instability of equal channel angular extruded T91 at ultra-high damage levels, *Acta Mater.* 132 (2017) 395–404, <https://doi.org/10.1016/j.actamat.2017.04.038>.
- [8] A. Hoffman, M. Arivu, H. Wen, L. He, K. Sridharan, X. Wang, W. Xiong, X. Liu, L. He, Y. Wu, Enhanced resistance to irradiation induced ferritic transformation in nanostructured austenitic steels, *Materialia* 13 (2020), 100806, <https://doi.org/10.1016/j.mtla.2020.100806>.
- [9] E. Aydogan, T. Chen, J.G. Gigax, D. Chen, X. Wang, P.S. Dzhumaev, O. V. Emelyanova, M.G. Ganchenkova, B.A. Kalin, M. Leontiva-Smirnova, R.Z. Valiev, N.A. Enikeev, M.M. Abramova, Y. Wu, W.Y. Lo, Y. Yang, M. Short, S.A. Maloy, F. A. Garner, L. Shao, Effect of self-ion irradiation on the microstructural changes of alloy EK-181 in annealed and severely deformed conditions, *J. Nucl. Mater.* 487 (2017) 96–104, <https://doi.org/10.1016/j.jnucmat.2017.02.006>.
- [10] J. Zhou, M.I. Islam, S. Guo, Y. Zhang, F. Lu, Radiation-induced grain growth of nanocrystalline $Al_x CoCrFeNi$ high-entropy alloys, *J. Phys. Chem. C* 125 (2021) 3509–3516, <https://doi.org/10.1021/acs.jpcc.0c09061>.
- [11] Z. Zhang, D.E.J. Armstrong, P.S. Grant, The effects of irradiation on CrMnFeCoNi high-entropy alloy and its derivatives, *Prog. Mater. Sci.* 123 (2022), 100807, <https://doi.org/10.1016/j.pmatsci.2021.100807>.
- [12] N.A.P.K. Kumar, C. Li, K.J. Leonard, H. Bei, S.J. Zinkle, Microstructural stability and mechanical behavior of FeNiMnCr high entropy alloy under ion irradiation, *Acta Mater.* 113 (2016) 230–244, <https://doi.org/10.1016/j.actamat.2016.05.007>.
- [13] K. Jin, C. Lu, L.M. Wang, J. Qu, W.J. Weber, Y. Zhang, H. Bei, Effects of compositional complexity on the ion-irradiation induced swelling and hardening in

- Ni-containing equiatomic alloys, *Scr. Mater.* 119 (2016) 65–70, <https://doi.org/10.1016/j.scriptamat.2016.03.030>.
- [14] C. Lu, T. Yang, K. Jin, G. Velisa, P. Xiu, M. Song, Q. Peng, F. Gao, Y. Zhang, H. Bei, W.J. Weber, L. Wang, Enhanced void swelling in NiCoFeCrPd high-entropy alloy by indentation-induced dislocations, *Mater. Res. Lett.* 6 (2018) 584–591, <https://doi.org/10.1080/21663831.2018.1504136>.
- [15] C.M. Barr, J.E. Nathaniel, K.A. Unocic, J. Liu, Y. Zhang, Y. Wang, M.L. Taheri, Exploring radiation induced segregation mechanisms at grain boundaries in equiatomic CoCrFeNiMn high entropy alloy under heavy ion irradiation, *Scr. Mater.* 156 (2018) 80–84, <https://doi.org/10.1016/j.scriptamat.2018.06.041>.
- [16] G. Pu, L. Lin, R. Ang, K. Zhang, B. Liu, B. Liu, T. Peng, S. Liu, Q. Li, Outstanding radiation tolerance and mechanical behavior in ultra-fine nanocrystalline Al_{1.5}CoCrFeNi high entropy alloy films under He ion irradiation, *Appl. Surf. Sci.* 516 (2020), 146129, <https://doi.org/10.1016/j.apsusc.2020.146129>.
- [17] G.S. Jawaharam, C.M. Barr, A.M. Monterrosa, K. Hattar, R.S. Averback, S. J. Dillon, Irradiation induced creep in nanocrystalline high entropy alloys, *Acta Mater.* 182 (2020) 68–76, <https://doi.org/10.1016/j.actamat.2019.10.022>.
- [18] T. Nagase, P.D. Rack, J.H. Noh, T. Egami, In-situ TEM observation of structural changes in nano-crystalline CoCrCuFeNi multicomponent high-entropy alloy (HEA) under fast electron irradiation by high voltage electron microscopy (HVEM), *Intermetallics* 59 (2015) 32–42, <https://doi.org/10.1016/j.intermet.2014.12.007>.
- [19] J. Gubicza, P.T. Hung, M. Kawasaki, J.-K. Han, Y. Zhao, Y. Xue, J.L. Lábár, Influence of severe plastic deformation on the microstructure and hardness of a CoCrFeNi high-entropy alloy: a comparison with CoCrFeNiMn, *Mater. Charact.* 154 (2019) 304–314, <https://doi.org/10.1016/j.matchar.2019.06.015>.
- [20] D.-H. Lee, I.-C. Choi, M. Kawasaki, T.G. Langdon, J. Jang, Nanomechanical behavior of high-entropy alloys processed by high- pressure torsion: a review, *Mater. Trans.* (Submitted).
- [21] B. Schuh, F. Mendez-Martin, B. Völker, E.P. George, H. Clemens, R. Pippan, A. Hohenwarter, Mechanical properties, microstructure and thermal stability of a nanocrystalline CoCrFeMnNi high-entropy alloy after severe plastic deformation, *Acta Mater.* 96 (2015) 258–268, <https://doi.org/10.1016/j.actamat.2015.06.025>.
- [22] X. Liu, J.-K. Han, Y. Onuki, Y.O. Kuzminova, S.A. Evlashin, M. Kawasaki, K.-D. Liss, Situ neutron diffraction investigating microstructure and texture evolution upon heating of nanostructured CoCrFeNi high-entropy alloy, *Adv. Eng. Mater.* (2023), 2201256, <https://doi.org/10.1002/adem.202201256>.
- [23] J.F. Ziegler, M.D. Ziegler, J.P. Biersack, SRIM – The stopping and range of ions in matter (2010), *Nucl. Instrum. Methods Phys. Res. Sect. B Beam Interact. Mater. At.* 268 (2010) 1818–1823, <https://doi.org/10.1016/j.nimb.2010.02.091>.
- [24] S.J. Zinkle, L.L. Snead, Opportunities and limitations for ion beams in radiation effects studies: bridging critical gaps between charged particle and neutron irradiations, *Scr. Mater.* 143 (2018) 154–160, <https://doi.org/10.1016/j.scriptamat.2017.06.041>.
- [25] G.M. Pharr, J.H. Strader, W.C. Oliver, Critical issues in making small-depth mechanical property measurements by nanoindentation with continuous stiffness measurement, *J. Mater. Res.* 24 (2009) 653–666, <https://doi.org/10.1557/jmr.2009.0096>.
- [26] K.P. Gupta, The Co-Ni-Sn (Cobalt-Nickel-Tin) System, *J. Phase Equilibria Diffus.* 30 (2009) 646–650, <https://doi.org/10.1007/s11669-009-9577-z>.
- [27] L. Tan, J.T. Busby, Formulating the strength factor α for improved predictability of radiation hardening, *J. Nucl. Mater.* 465 (2015) 724–730, <https://doi.org/10.1016/j.jnucmat.2015.07.009>.
- [28] Z. Wu, H. Bei, G.M. Pharr, E.P. George, Temperature dependence of the mechanical properties of equiatomic solid solution alloys with face-centered cubic crystal structures, *Acta Mater.* 81 (2014) 428–441, <https://doi.org/10.1016/j.actamat.2014.08.026>.
- [29] N. Hansen, Hall-Petch relation and boundary strengthening, *Scr. Mater.* 51 (2004) 801–806, <https://doi.org/10.1016/j.scriptamat.2004.06.002>.
- [30] N. Hansen, X. Huang, D.A. Hughes, Microstructural evolution and hardening parameters, *Mater. Sci. Eng. A* 317 (2001) 3–11, [https://doi.org/10.1016/S0921-5093\(01\)01191-1](https://doi.org/10.1016/S0921-5093(01)01191-1).
- [31] P.T. Hung, M. Kawasaki, J.-K. Han, Á. Szabó, J.L. Lábár, Z. Hegedüs, J. Gubicza, Thermal stability of nanocrystalline CoCrFeNi multi-principal element alloy: effect of the degree of severe plastic deformation, *Intermetallics* 142 (2022), 107445, <https://doi.org/10.1016/j.intermet.2021.107445>.
- [32] Yu. Ivanisenko, R.Z. Valiev, H.-J. Fecht, Grain boundary statistics in nano-structured iron produced by high pressure torsion, *Mater. Sci. Eng. A* 390 (2005) 159–165, <https://doi.org/10.1016/j.msea.2004.08.071>.
- [33] W. Skrotzki, A. Pukenas, E. Odor, B. Joni, T. Ungar, B. Völker, A. Hohenwarter, R. Pippan, E.P. George, Microstructure, texture, and strength development during high-pressure torsion of CrMnFeCoNi high-entropy alloy, *Crystals*. 10 (2020) 336, <https://doi.org/10.3390/crys10040336>.
- [34] T.S. Reddy, I.S. Wani, T. Bhattacharjee, S.R. Reddy, R. Saha, P.P. Bhattacharjee, Severe plastic deformation driven nanostructure and phase evolution in a Al 0.5 CoCrFeMnNi dual phase high entropy alloy, *Intermetallics* 91 (2017) 150–157, <https://doi.org/10.1016/j.intermet.2017.09.002>.